

Journal of Materials Chemistry A

Accepted Manuscript



This is an *Accepted Manuscript*, which has been through the Royal Society of Chemistry peer review process and has been accepted for publication.

Accepted Manuscripts are published online shortly after acceptance, before technical editing, formatting and proof reading. Using this free service, authors can make their results available to the community, in citable form, before we publish the edited article. We will replace this *Accepted Manuscript* with the edited and formatted *Advance Article* as soon as it is available.

You can find more information about *Accepted Manuscripts* in the [Information for Authors](#).

Please note that technical editing may introduce minor changes to the text and/or graphics, which may alter content. The journal's standard [Terms & Conditions](#) and the [Ethical guidelines](#) still apply. In no event shall the Royal Society of Chemistry be held responsible for any errors or omissions in this *Accepted Manuscript* or any consequences arising from the use of any information it contains.

High N-content holey few-layered graphene electrocatalysts: scalable solvent-less production

Cite this: DOI: 10.1039/x0xx00000x

Dan Liu,^a Weiwei Lei,^{a*} David Portehault,^b Si Qin^a and Ying (Ian) Chen^{a*}

Received 00th January 2012,
Accepted 00th January 2012

DOI: 10.1039/x0xx00000x

www.rsc.org/

Few layered nitrogen doped graphene (NG) attracts great interest in energy storage and conversion applications due to its electronic and catalytic properties. However, its bulk production cannot be envisioned by current synthetic methods. Here we report a facile, solvent-less, low cost and high yield process towards NG. Mechanochemical solid-state exfoliation allows scalable synthesis of holey and crumple nitrogen-doped few-layered graphene from graphite with controlled high concentration N doping and a high surface area, through ball-milling. By adjusting the ratio of starting materials, the nitrogen content can be modulated from 4.87 to 17.83 at.%. Furthermore, the types of nitrogen-containing species in few-layered graphene can also be controlled. The resultant NG exhibited superior oxygen reduction reaction (ORR) performance and more reliable stability than commercial Pt/C catalyst.

Introduction

Graphene, a single sheet of carbon atoms packed in a honeycomb lattice, offers great potential for various applications, including nanoelectronics,^{1,2} energy conversion and storage,^{3,4} electrocatalysis⁵ and sensors^{6,7} due to its unique electronic and mechanical properties. Developing simple methods for the large-scale synthesis of graphene has been intensively explored in recent years. Up to now, there are three main strategies for preparing large-area and high-quality graphene including large-scale growth, *i.e.* chemical vapor deposition (CVD)^{8,9}, chemical reduction of graphite oxide (GO)¹⁰⁻¹² and exfoliation (e.g., liquid-exfoliation of intercalated graphite¹³). CVD involves metal catalysts or foils, such as nickel and copper, and stringent fabrication conditions. CVD is tedious and expensive for large-scale production but allows production of high quality pure graphene, relevant for electronics for instance. Such grade is however not needed for other applications, especially those related to catalysis. In this case, the synthesis of GO for chemical reduction usually involves strong, hazardous oxidizing reagents (e.g., KMnO₄ and H₂SO₄), excessive sonication and centrifugation, and a complicated multistep process.^{10,11} Furthermore, the reduction reaction for synthesis of graphene also requires hazardous reducing reagents (e.g., NaBH₄).¹² On the other hand, the liquid-exfoliation method usually suffers from a mutli-step process involving strong sonication, excessive centrifugation, and the need for appropriate solvents, which are usually expensive and toxic. Ball milling has been envisaged to

circumvent these obstacles but usually results in poor yield and high dispersion in terms of the number of stacked layers.¹⁴⁻¹⁹ Thus, the development of a simple and solid-phase method to produce crumpled graphene in high yield is urgently required.

So far, both theoretical and experimental studies have demonstrated that the Fermi level of graphene can be further fine-tuned by doping, especially by nitrogen, showing excellent electrochemical properties as carbocatalysts and toward the oxygen reduction reaction (ORR), lithium ion batteries, supercapacitors and dye-sensitized solar cells applications.²⁰⁻²⁶ In addition, it is well known that the electronic properties of doped graphene are strongly linked to the dopant concentration.²⁷ However, most of the current methods of synthesizing NG face some issues like starting from GO requiring strong and hazardous oxidizing reagents, low yield production, uncontrolled and low-concentration nitrogen doping. Therefore, the search for a low-cost, efficient, and scalable synthetic method toward N-doped graphene in a controlled manner is highly challenging and desirable.

Herein we report a simple, effective and large-scale approach for the synthesis of NG with controlled high N concentration based on solid-state exfoliation of graphite by ball milling. In this synthesis guanidine hydrochloride (GH) is solely added for the *in situ* exfoliation of graphite, and as N source. This approach is also facile for gradually tuning the concentration of nitrogen in a wide range from 4.9 to 17.8 at.% with maintained morphology. A comparison with the well-known Hummer's method (HM) pleads in the advantage of this new solid-state exfoliation method in terms of yield and simplicity. The as-

synthesized NG with crumple and holey nanostructures exhibit remarkable catalytic activity for the oxygen reduction reaction depending on the nitrogen-containing species. These metal-free electrocatalysts also show good tolerance to the methanol crossover effect and excellent long-term stability.

Experimental

Material synthesis

In a typical synthesis, graphite and GH with different weight ratios (1:100, 1:200, 1:300, and 1:400, respectively) were mixed together inside a steel milling container (Pulverisette 7, Fritsch) at a rotation speed of 700 rpm for 20h at room temperature under nitrogen atmosphere. The mixture powders were then loaded into a quartz boat and then heated to 800 °C at 10 °C/min with a 1h dwell time under a nitrogen flow in a tubular oven connected to a basic water bubbler. The latter is used for the sake of precautions to trap potentially harmful gases (see main text and caption of Figure S4). After the heating process, black NG samples were produced in a large scale, only a small weight gain/loss relative to the amount of graphite used due to the loss of carbon during annealing or the gain of carbon (and nitrogen) atoms from GH (for example, 119 mg NG100 versus 120 mg graphite and 12 g GH, 58.5 mg NG200 versus 60 mg graphite and 12 g GH, 40.2 mg NG300 versus 40 mg graphite and 12g GH, and 30.5 mg NG400 versus 30 g graphite and 12 g GH).

Characterization

The as-synthesized samples were examined using X-ray powder diffraction (XRD) (Panalytical X'Pert PRO system) using Cu K α radiation. TGA was performed on a Netzsch STA409PC/PG apparatus under nitrogen flow with a 10 °C min⁻¹ heating rate. X-ray photoelectron spectroscopy (XPS) was employed using an ESCALAB 250 instrument equipped with using non-monochromatised Mg-K α X-ray as the excitation source. Raman measurement was performed on a Renishaw Raman spectrometer with a laser wavelength of 514.5 nm at room temperature. The sample morphology were characterized using a Zeiss Supra 55 VP SEM. Transmission electron microscopy (TEM) was performed on a JEOL 2100F (operating at 200 kV) apparatus. The AFM measurements were performed on a Cypher atomic force microscope. Nitrogen adsorption and desorption isotherms were obtained using a Tristar 3000 apparatus at 77 K.

Electrochemical characterization

The ORR performances of the catalysts were evaluated on an electrochemical workstation (Solartron 1470E) with a typical three-electrode cell. All the experiments were conducted at ambient condition. The potentials presented in this study are referred to as standard hydrogen electrode (SHE). The potential is 0.098 V versus SHE with respect to the electrodes Hg/HgO. 5 mg of the NG samples were dispersed in a solution containing 0.9 ml of ethanol and 0.1 ml of 5 wt % Nafion solution. The mixture was ultrasonicated to obtain a homogenous catalyst ink. The

working electrodes were fabricated by pasting 10 μ L aliquot of this catalyst ink on a glassy carbon rotating disk electrode (5 mm in diameter, from PINE Instruments, USA). The catalyst loading was 50 μ g (0.255 mg/cm²) on the electrode. For comparison, 1 mg commercial Pt/C (20 wt % Pt) catalyst was dispersed in 1 mL ethanol/Nafion solution. The electrode was fabricated by the same procedure described above, which leads to a mass loading of 10 μ g (0.051 mg/cm²) and a comparable current density to the N doped few-layered graphene. The electrolyte was 0.1 M KOH solution, the counter- and the reference electrodes were a platinum wire and an Hg/HgO electrode, respectively. Cyclic voltammetry was performed from 0.2 to -0.8 V (vs SHE) at 50 mV s⁻¹ after purging the electrolyte with N₂ or O₂ gas for 1 h. Linear-scan-voltammetry (LSV) measurements were performed by using the RDE at different rotating speeds from 400 to 2500 rpm in an O₂-saturated electrolyte from 0.2 to -0.8 V (vs SHE) at a sweep rate of 5 mV S⁻¹. The electrode was then scanned in an N₂-saturated electrolyte in the same conditions to evaluate the background capacitance current. The oxygen reduction current was evaluated after subtracting the capacitive current.

Results and discussion

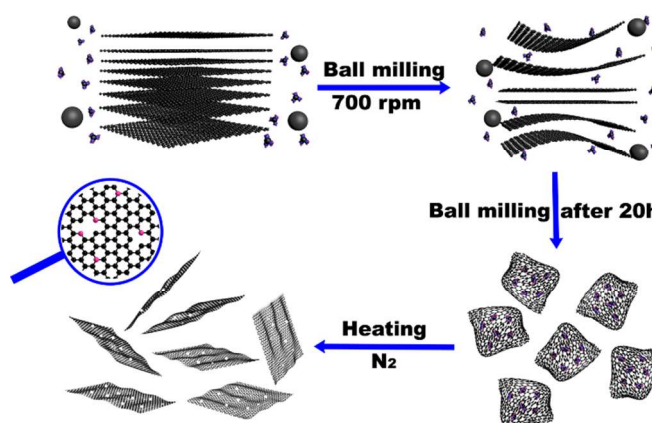


Figure 1. Schematic of the synthetic process that involves milling of graphite with GH particles to form graphene-wrapped GH particles, followed by annealing at 800 °C to achieve nitrogen-doped few-layered graphene.

The synthetic procedure is illustrated in Figure 1. Firstly, GH particles were intercalated between the graphite layers thanks to kinetic energy provided by ball milling to cause edge-opened graphite. It was confirmed by the X-ray diffraction (XRD) patterns of the intermediate products after 5h and 10h milling (Figure S1 in Supporting information) that show dramatically broadened (002) reflections. An excess of GH over graphite was used to ensure that sufficient particles of GH were intercalated into the layers of graphite. Upon further milling, graphite was exfoliated into few layers to form fully graphene-wrapped GH particles according to TEM (Figure S2). Finally, the composite was heated at 800 °C under flowing N₂ for 1h. During this step, GH underwent polymerisation followed by

complete thermolysis at 800 °C according to thermogravimetric analysis (TGA, Figure S3). The reaction was monitored by TEM and TGA coupled to mass spectrometry to analyse gases evolving in the course of calcination. The reaction mechanism is similar to pure guanidine-HCl decomposition (Figure S4). Upon temperature increase, 3 mass losses of 56, 14 and 39% occur in the ranges 290-390 °C, 400-500 °C and 600-750 °C, respectively. The first two losses are mainly associated with HCl and NH₃ evolution and correspond to guanidine polycondensation²⁸ with *in situ* formation of g-C₃N₄, in agreement with the yellowish color and the XRD pattern of the powder recovered at 450 °C (Figure S5). An intimate graphene/g-C₃N₄ is then obtained at this stage where graphene layers are separated by *in situ* formed carbon nitride. The third mass loss relates to decomposition of g-C₃N₄ and evolution of C₂N₂, NHCHNH₂ and HCl from chloride remaining in the structure. Upon carbon nitride decomposition, graphene sheets are maintained separated. In addition, the evolved gaseous N-rich species may act as reagents for N-functionalization of the graphene sheets.

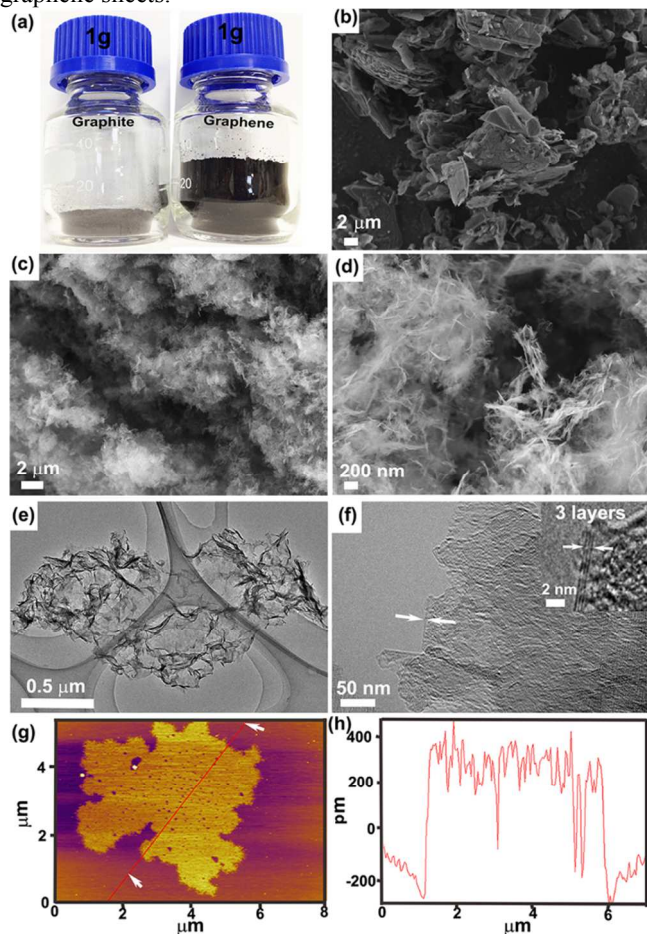


Figure 2. (a) Example of the bulk quantity of graphene product compared with initial graphite. The image consists of approximately 1 g of sample. (b, c) Low-magnification SEM image of graphite and NG400, respectively. (d) High-magnification SEM image of crumpled NG. (e) TEM image of a single few-layered graphene showing holes and crumple structure. (f) High-resolution TEM image of NG. The inset shows the edge folding of a graphene sheets with three layers domains

highlighted by white arrows. (g) High-magnification AFM image of a NG. The holey structure can be seen clearly. (h) The height profiles showing typical size and thickness of a single graphene.

A series of NG samples denoted as NG_x, where x stands for the initial weight ratio of graphite and GH (1:100, 1:200, 1:300, 1:400), were investigated. XRD (Figure S6) shows that all samples are structurally similar, without any detectable impurity. All samples were obtained on gram scale without any post-purification or separation processes, as shown in Figure 2a. Compared with graphite (Figure 2b), a fluffy and lamellar morphology can be seen from the scanning electron microscopy (SEM) images of NG400 (Figure 2c). This typical crumpling and flexibility of few layered graphene is observed in each NG_x samples (Figures 2d and S7-9). Figure 2e presents transmission electron microscopy (TEM) image of NG400, in which a crumpled and holey structure can be discerned. The NG400 was further characterized by element mapping of carbon and nitrogen (Figure 3). Nitrogen appears as homogeneously distributed in the NG sheets. High-resolution TEM (HRTEM, Figure 2f) at the edge of NG400 shows three parallel fringes corresponding to three stacked layers in the sample. Atomic force microscopy (AFM) images (Figure 2g,h) evidences the layered structure with a uniform thickness of 0.6 nm indicating two stacked layers. The thickness distribution was statistically evaluated by AFM and SEM measurements on 100 sheets (Figure S10). The NG thickness was mostly below 5 nm, a few sheets were around 10 nm-thick. AFM further reveals that the NG400 sheets have a holey structure (Figure 2g,h). Such nano-holes may originate from the gases evolving during GH thermolysis. The porosity of the materials was studied by nitrogen sorption (Figure S11). The specific surface areas derived from the Brunauer–Emmet–Teller (BET) method are 145, 253, 281 and 366 m²g⁻¹ for NG100, NG200, NG300 and NG400, respectively. Such relatively high surface area could contribute to the ORR activity of NG_x samples.

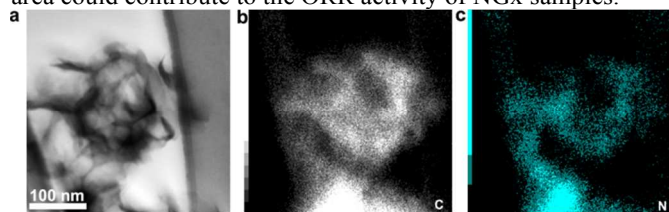


Figure 3. (a) TEM image of NG400. Corresponding element mappings of (b) carbon and (c) nitrogen, respectively.

X-ray photoelectron spectroscopy (XPS, Figure S12) confirms the presence of carbon and nitrogen. The C1s peaks centered at 284.7 and 288.1 eV (Figure 4a) can be ascribed to sp² C=C bond and sp³ C-N bond, respectively.²⁹ Three peaks centered at 398.9, 399.8, and 400.9 eV in the N1s spectrum (Figure 4b) correspond to pyridinic, pyrrolic and quaternary N, respectively.³⁰⁻³¹ Pyridinic and pyrrolic N are bonded to two adjacent carbon atoms at the edges and defect sites of the graphene plane.³² Quaternary N usually substitutes for carbon and bonds with three sp² hybridized C neighbors (Figure 4c).³³ The N doping concentration (Figure 4) reaches its maximum (17.83 at.%) in NG400, and then decreases with the reducing

weight ratio of GH versus graphite with 11.99, 8.32 and 4.87 at.% for NG300, NG200 and NG100, respectively. Nitrogen atoms are mainly in the forms of pyridinic and pyrrolic N (Figure 4). In contrast, quaternary N only accounts for 9–13% of the N species in all NGx. It has been reported that the pyridinic and pyrrolic N are ORR-active catalysts in NG, which indicate that our samples are very attractive for ORR catalytic activity, especially for the NG400 with a high nitrogen doping level.^{34,35}

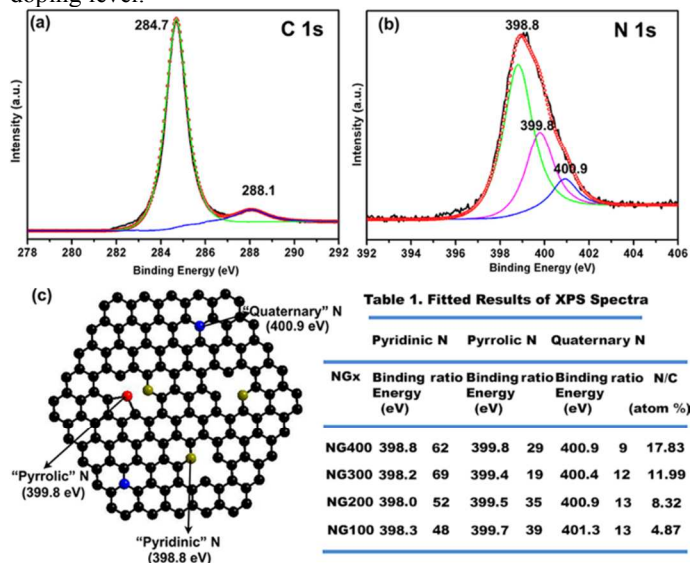


Figure 4. High-resolution C1s (a) and N1s (b) XPS spectra of NG400. (c) Scheme of three types (pyridine, pyrrolic, and quaternary) of nitrogen in NG.

Raman spectroscopy is another efficient method to characterize the structure and quality of NG. The Raman spectra (Figure 5) of NGx display the characteristic signals of the D and G bands around 1350 and 1582 cm^{-1} as well as two weak D' and 2D bands at 1630 and 2718 cm^{-1} , well matching previously reported data.³⁶ Both D and D' bands originate from the intervalley double-resonance scattering process. Especially, the D band is activated by defects i.e., in-plane substitution heteroatoms, vacancies, or grain boundaries/edges.³⁷ The high relative intensity of D and D' bands in the spectra of NGx indicate large amount of defects in NGx induced by nanoscaling and the incorporated nitrogen atoms, further confirming the successful doping of graphene sheets.³⁸ The G band is attributed to the optical E_{2g} phonons at the Brillouin zone center, related to phonon vibrations in the sp^2 framework. Different from the D band, the 2D band always can be seen in Raman spectra of graphene due to same intervalley double-resonance scattering of two TO phonons around the K-point of the Brillouin zone but does not require the activation of defects. Generally, the intensity ratio of D band to G band (I_D/I_G) can be used to estimate the doping level. To take into account potential inhomogeneous distribution of defects in NGx, Raman spectra were investigated at three different dots for each sample. As shown in Figure 5, value of I_D/I_G increases from 0.85 to 1.29 with the increasing weight ratio of graphite and GH. This suggests that a relatively high defects and edge plane exposure in NG400 caused by the introduction of more nitrogen atoms, which is consistent with the results of XPS. In addition, the D band and G band display blue shift from NG100 to NG400. These should be caused by the different bond distances in C-C and C-N bonds, which further provide the evidence of N doping in our sample.

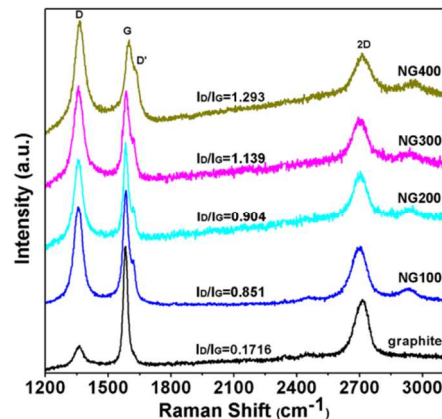


Figure 5. Comparison of Raman spectra for graphite and as-prepared NGx using a 514.5 nm line of an argon ion laser.

To gain insight into the metal free catalytic behavior of NGx, oxygen reduction reaction (ORR) in 0.1 M KOH solution was evaluated using cyclic voltammetry at a scan rate of 50 mV s^{-1} . Figure S13 shows obvious oxygen reduction peaks for all NGx electrodes in the O_2 -saturated solution, indicating catalytic activity. The linear sweep voltammeteries (LSVs) curves of NG400 under various electrode rotating speeds using rotating disk electrode are shown in Figure 6a. The current density was increased with the rotating speed due to the reduced diffusion length. The number of electrons transferred per O_2 molecule is evaluated at 3.66 from the slope of the Koutecky-Levich plot³⁹ (insert Figure 6a), in good agreement with an ideal four-electron reduction from O_2 to H_2O . Another important criterion to evaluate the activity of an electrocatalyst is the onset potential of the ORR. The corresponding values are much higher for all NGx than original graphite and increased gradually with increasing N content (Figure 6b and Figure S14): Graphite (-0.01 V) < NG100 < (0.08 V) < NG200 (0.10 V) < NG300 (0.12 V) < NG400 (0.15 V). NG400 appears as a superior ORR catalyst as its onset potential is only 40 mV below that of Pt/C (0.19 V). Our results support the conclusions of recent reports which have suggested that both pyridinic and pyrrolic N play a major role in the enhanced ORR activity of N-doped carbons.^{34,35,40,41}

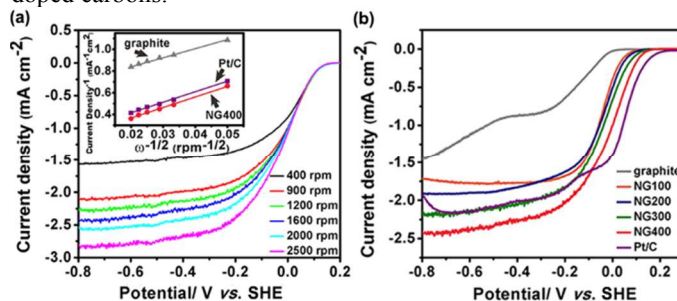


Figure 6. (a) Rotating disk electrode (RDE) linear sweep voltammograms of NG400 in O_2 -saturated 0.1 M KOH with various rotation rates at a scan rate of 5 mV s^{-1} . The inset shows Koutecky–Levich plots of graphite, NG400, and Pt/C derived from RDE measurements at different electrode potentials. (b) RDE voltammograms of graphite, NG100, NG200, NG300, NG400, and Pt/C at a rotation rate of 1600 rpm.

Furthermore, the NG400 sample shows a remarkable tolerance for methanol cross-over effect (Figure 7) and excellent long term durability (Figure 8), which are superior to Pt/C and therefore endow it a promising candidate for fuel cells. These results indicate that the enhanced electrochemical activities for ORR of NGx should result from the high-concentration nitrogen doping, holey and crumple structure, and large surface area.

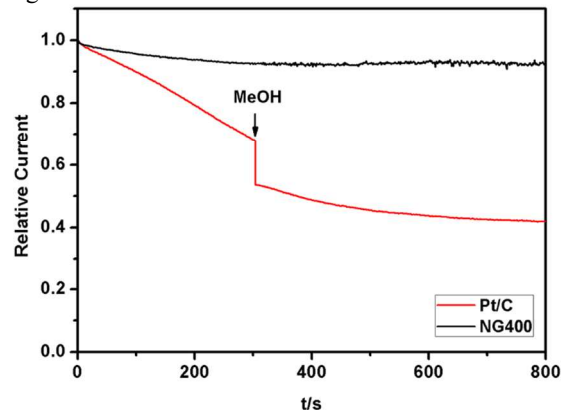


Figure 7. Chronoamperometric measurement for NG400 and Pt/C electrocatalysts in an O₂-saturated 0.1 M KOH solution and 3.0 M methanol were added at around 300 s at 1600 rpm.

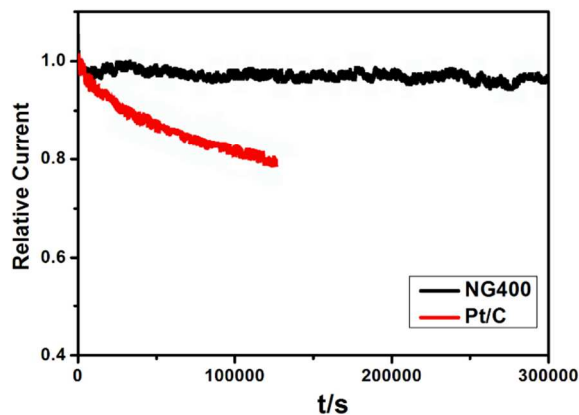


Figure 8. Current-time chronoamperometric response of NG400 and Pt/C catalysts at -0.3 V in O₂ saturated aqueous solution of 0.1 M KOH at a rotation rate of 1600 rpm.

To date, many methods for the synthesis of NG have been reported. However, these techniques do not provide easy control of the nitrogen concentration and require strict conditions, including multistep processes, solvents and large footprint apparatuses (SI). It has been reported that ball milling is a facile, economical and eco-friendly method for synthesizing graphene.¹⁴⁻¹⁹ In our work, we used environmental benign graphite and guanidine hydrochloride as reagents to synthesize NG with high N concentration and good selectivity toward few-layered graphene, without involving any catalyst, template or solvent. The difference in terms of selectivity versus previously reported procedures may originate from the use of a specific reactant that could intercalate efficiently between the graphene sheets and strongly enhance the

exfoliation process. Besides, our ball milling method shows high power with a speed of rotation as high as 700 rpm, which may provide enough energy for exfoliating graphite into few-layered graphene. Importantly, this “mechanochemical solid-state exfoliation” is more efficient in terms of yield and simplicity (quantitative yield vs. 30% for HM, see SI). In addition, the procedure also enables facile adjustment of the doping level.

To understand the role of ball milling in the synthesis of nitrogen-doped few-layered graphene, a sample was prepared only by heating the mixture of graphite and GH without ball milling. As shown from XRD, SEM and the ORR activity (Figures S15-17), no exfoliation is evidenced and the bulk particles show poor ORR activity. Therefore, ball milling is mandatory to provide enough energy through collisions for GH intercalation between graphene layers to ensure further exfoliation. Interestingly, GH not only acts as the N source and sacrificial template for the solid-exfoliation, but also supports the formation of holey and crumple structure, presumably due to the released gas species.

Conclusions

In summary, we have developed a new simple, efficient and scalable mechanical solid-state exfoliation approach based on ball milling for the synthesis of holey and crumple NG with controlled N content and promising electrocatalytic performances. These results represent an important step toward large-scale NG synthesis, while mechanical solid-state exfoliation could be further extended to pave the way to new 2D nanomaterials with large surface and controlled doping.

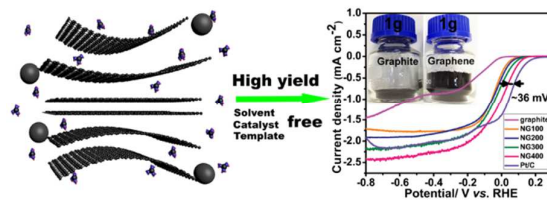
Acknowledgements

Financial support from the Australian Research Council under the Centre of Excellence program and DECRA Research Fellowship, and Central Research Grant Scheme (CRGS) from Deakin University are acknowledged.

Notes and references

- ^a Institute for Frontier Materials, Deakin University, Waurn Ponds, Victoria 3216, Australia
E-mail: weiwei.lei@deakin.edu.au; ian.chen@deakin.edu.au
 - ^b Sorbonne Universités, UPMC Univ Paris 06 – CNRS – Collège de France UMR 7574, Chimie de la Matière Condensée de Paris F-75005, Paris, France
- †Electronic Supplementary Information (ESI) available: TGA, XRD, additional XPS spectra, SEM and TEM images. See DOI: 10.1039/b000000x/
- 1 K. S. Novoselov, A. K. Geim, S. V. Morozov, D. Jiang, M. I. Katsnelson, I. V. Grigorieva, S. V. Dubonos and A. A. Firsov, *Nature*, 2005, **438**, 197-200
 - 2 S. Wang, P. K. Ang, Z. Q. Wang, A. L. L. Tang, J. T. L. Thong and K. P. Loh, *Nano Letters*, 2010, **10**, 92–98.

- 3 W. Y. Tsai, R. Y. Lin, S. Murali, L. L. Zhang, J. K. McDonough, R. S. Ruoff, P. L. Taberna, Y. Gogotsi and P. Simon, *Nano Energy*, 2013, **2**, 403–411.
- 4 H. Hu, Z. B. Zhao, W. Wan, Y. Gogotsi and J. S. Qiu, *Advanced Materials*, 2013, **25**, 2219–2223.
- 5 Z. H. Sheng, L. Shao, J. J. Chen, W. J. Bao, F. B. Wang and X. H. Xia, *ACS Nano*, 2011 **5**, 4350–4358.
- 6 J. T. Robinson, F. K. Perkins, E. S. Snow, Z. Q. Wei and P. E. Sheehan, *Nano Letters*, 2008, **8**, 3137–3140;
- 7 C. H. Lu, H. H. Yang, C. L. Zhu, X. Chen and G. N. Chen, *Angewandte Chemie International Edition*, 2009, **48**, 4785–4787.
- 8 K. S. Kim, Y. Zhao, H. Jang, S. Y. Lee, J. M. Kim, K. S. Kim, J. H. Ahn, P. Kim, J. Y. Choi and B. H. Hong, *Nature*, 2009, **457**, 706–710.
- 9 A. Reina, X. T. Jia, J. Ho, D. Nezich, H. B. Son, V. Bulovic, M. S. Dresselhaus and J. Kong, *Nano Letters*, 2009, **9**, 30–35.
- 10 D. Li, M. B. Müller, S. Gilje, R. B. Kaner and G. G. Wallace, *Nature Nanotechnology*, 2008, **3**, 101 – 105.
- 11 S. Niyogi, E. Bekyarova, M. E. Itkis, J. L. McWilliams, M. A. Hamon and R. C. Haddon, *Journal of the American Chemical Society*, 2006, **128**, 7720–7721.
- 12 M. Feng, R. Q. Sun, H. B. Zhan and Y. Chen, *Nanotechnology*, 2010, **21**, 075601.
- 13 X. L. Li, G. Y. Zhang, X. D. Bai, X. M. Sun, X. R. Wang, E. G. Wang and H. J. Dai, *Nature Nanotechnology*, 2008, **3**, 538–542.
- 14 R. Aparna, N. Sivakumar, A. Balakrishnan, A. S. Nair, S. V. Nair, K. R. V. Subramanian, *J. Renew. Sustain. Energy*, 2013, **5**, 033123–
- 15 A. E. D. Rio-Castillo, C. Merino, E. Diez-Barra and E. Vazquez, *Nano Research*, 2014, **7**, 963–972.
- 16 M. Mao, S. Z. Chen, P. He, H. L. Zhang and H. T. Liu, *J. Mater. Chem. A*, 2014, **2**, 4132–4135
- 17 V. Leon, A. M. Rodriguez, P. Prieto, M. Prato and E. Vazquez, *ACS Nano*, 2014, **8**, 563–571
- 18 I. Y. Jeon, Y. R. Shin, G. J. Sohn, H. J. Choi, S. Y. Bae, J. Mahmood, S. M. Jung, J. M. Seo, M. J. Kim, D. W. Chang, L. M. Dai and J. B. Baek, *Proceedings of the National Academy of Sciences*, 2012, **109**, 5588–5593.
- 19 I. Y. Jeon, H. J. Choi, M. J. Ju, I. T. Choi, K. Lim, J. Ko, H. K. Kim, J. C. Kim, J. J. Lee, D. Shin, S. M. Jung, J. M. Seo, M. J. Kim, N. Park, L. M. Dai and J. B. Baek, *Scientific reports*, 2013, **3**, 2260.
- 20 Z. H. Wen, X. C. Wang, S. Mao, Z. Bo, H. Kim, S. M. Cu, G. H. Lu, X. L. Feng and J. H. Chen, *Advanced Materials*, 2012, **24**, 5610–5616;
- 21 H. B. Wang, C. J. hang, Z. H. Liu, L. Wang, P. X. Han, H. X. Xu, K. J. Zhang, S. M. Dong, J. H. Yao and G. L. Cui, *Journal of Material Chemistry*, 2011, **21**, 5430–5434;
- 22 Y. Zheng, Y. Jiao, L. Ge, M. Jaroniec and S. Z. Qiao, *Angewandte Chemie International Edition*, 2013, **125**, 3192–3198.
- 23 X. H. Li and M. Antonietti, *Angewandte Chemie International Edition*, 2013, **52**, 4572 –4576.
- 24 X. H. Li, S. Kurasch, U. Kaiser and M. Antonietti, *Angewandte Chemie International Edition*, 2012, **51**, 9689 –9692.
- 25 J. Liang, Y. Jiao, M. Jaroniec and S. Z. Qiao, *Angewandte Chemie International Edition*, 2012, **51**, 11496–11500
- 26 Y. H. Xue, J. Liu, H. Chen, R. G. Wang, D. Q. Li, J. Qu and L. M. Dai, *Angewandte Chemie International Edition*, 2012, **51**, 12124 – 12127.
- 27 L. Y. Zhao, R. He, K. T. Rim, T. Schiros, K. S. Kim, H. Zhou, C. Gutierrez, S. P. Chockalingam, C. J. Arguello, L. Plov, D. Nordlund, M. S. Hybertsen, D. R. Reichman, T. F. Heinz, P. Kim, A. Pinczuk, G. W. Flynn and A. N. Pasupathy, *Science*, 2011, **333**, 999–1003.
- 28 J. Xu, H.-T. Wu, X. Wang, B. Xue, Y.-X. Li and Y. Cao, *Physical Chemistry Chemical Physics*, 2013, **15**, 4510–4517.
- 29 D. Wei, Y. Liu, Y. Wang, H. Zhang, L. Huang and G. Yu, *Nano Letters*, 2009, **9**, 1752–1758.
- 30 C. Zhang, L. Fu, N. Liu, M. Liu, Y. Wang and Z. Liu, *Advanced Materials*, 2011, **23**, 1020–1024;
- 31 H. B. Wang, T. Maiyalagan and X. Wang, *ACS Catalysis*, 2012, **2**, 781–794.
- 32 H. T. Chung, J. H. Won and P. Zelenay, *Nature Communications*, 2013, **4**, 1922.
- 33 S. Hou, X. Cai, H. Wu, X. Yu, M. Peng, K. Yan and D. Zou, *Energy & Environmental Science*, 2013, **6**, 3356–3362.
- 34 Ya. Zhao, C. G. Hu, Y. Hu, H. H. Cheng, G. Q. Shi and L. T. Qu, *Angewandte Chemie International Edition*, 2013, **124**, 11533 –11537
- 35 S. Yu, D. Q. Zhang and L. M. Dai, *Journal of the American Chemical Society*, 2010, **132**15127.
- 36 T. Xing, L. H. Li, L. T. Hou, X. P. Hu, S. X. Zhou, R. Peter, M. Petravic and Y. Chen, *Carbon*, 2013, **57**, 515–519.
- 37 L. M. Malard, M. A. Pimenta, G. Dresselhaus and M. S. Dresselhaus, *Physics Reports*, 2009, **473**, 51–87.
- 38 H. B. Wang, C. J. hang, Z. H. Liu, L. Wang, P. X. Han, H. X. Xu, K. J. Zhang, S. M. Dong, J. H. Yao and G. L. Cui, *Journal of Material Chemistry*, 2011, **21**, 5430–5434.
- 39 X. F. Liu and M. Antonietti, *Advanced Materials*, 2013, **25**, 6284–6290.
- 40 S. B. Yang, X. L. Feng, X. C. Wang and K. Müllen, *Angewandte Chemie International Edition*, 2011, **123**, 5339–5343.
- 41 R. L. Liu, D. Q. Wu, X. L. Feng and K. Müllen, *Angewandte Chemie International Edition*, 2010, **122**, 2619–2623.



High N-content (4.87 to 17.83 at.%) holey few-layered graphene was synthesized by a facile, solvent-less, low cost and high yield process.